An orthophosphate semiconductor with photooxidation properties under visible-light irradiation

Zhiguo Yi[1,2], Jinhua Ye[1]*, Naoki Kikugawa[1], Tetsuya Kako[1], Shuxin Ouyang[1], Hilary Stuart-Williams[3], Hui Yang[2], Junyu Cao[1], Wenjun Luo[4], Zhaosheng Li[4], Yun Liu[2] and Ray L. Withers[2]

The search for active semiconductor photocatalysts that directly split water under visible-light irradiation remains one of the most challenging tasks for solar-energy utilization[1-6]. Over the past 30 years, the search for such materials has focused mainly on metal-ion substitution as in $In_{1-x}Ni_xTaO_4$ and (V-, Fe- or Mn-)TiO_2 (refs 7,8), non-metal-ion substitution as in $TiO_{2-x}N_x$ and $Sm_2Ti_2O_5S_2$ (refs 9,10) or solid-solution fabrication as in $(Ga_{1-x}Zn_x)(N_{1-x}O_x)$ and $ZnS-CuInS_2-AgInS_2$ (refs 11,12). Here we report a new use of Ag_3PO_4 semiconductor, which can harness visible light to oxidize water as well as decompose organic contaminants in aqueous solution. This suggests its potential as a photofunctional material for both water splitting and waste-water cleaning. More generally, it suggests the incorporation of p block elements and alkali or alkaline earth ions into a simple oxide of narrow bandgap as a strategy to design new photoelectrodes or photocatalysts.

It is known that the photolysis of water using semiconductors involves photogenerated electrons and holes migrating to the surface of the semiconductor and serving as redox sources that then react with adsorbed water, leading to the splitting of water. Both light absorption and suitable redox potentials are prerequisites for the direct splitting of water. As semiconductors with suitable redox potentials are rare and redox power is weakened by bandgap narrowing, a widely used approach is to treat the water splitting reaction in terms of two coupled half-reactions[5,6,10,12–14]. This emphasizes the significance of developing visible-light-sensitive photofunctional materials with the alternative ability to evolve H_2 or O_2 from aqueous solutions containing sacrificial reagents. They can later be combined to form a complete water splitting system. Different compounds have been explored for this purpose. Water oxidation is found to be more challenging because the formation of one molecular oxygen involves the transportation and reaction of four electrons or holes[5,15].

The silver orthophosphate used in this study was prepared by a simple ion-exchange method in the case of the powder samples and by an *in situ* electrochemical deposition method in the case of the thin-film samples. The crystal structure of the material was first investigated in 1925 when Wyckoff established it as having a cubic structure type[16]. Later, as a result of progress in the X-ray diffraction (XRD) technique as well as the interest in the ionic conductivity of Ag_3PO_4 (refs 17,18), more accurate

crystal structures involving the determination of the silver and phosphorus fractional coordinates were established. Ag_3PO_4 is of body-centred cubic structure type with a lattice parameter of ∼6.004 Å (ref. 17). The structure consists of isolated, regular PO_4 tetrahedra (P–O distance of ∼1.539 Å) forming a body-centred cubic lattice. Six Ag^+ ions are distributed among twelve sites of two-fold symmetry. XRD patterns of our samples (see Fig. 1a) confirmed this crystal structure. The particle size of the crystals was estimated to be ∼0.5–2 μm from scanning electron microscopy (SEM) images such as that shown in Fig. 1b. The ultraviolet–visible diffuse reflectance spectrum (Fig. 1c) indicated that the golden coloured Ag_3PO_4 can absorb solar energy with a wavelength shorter than ∼530 nm. Further analysis of the absorption spectrum revealed an indirect bandgap of 2.36 eV as well as a direct transition of 2.43 eV (see Supplementary Fig. S1). The bandgap satisfies the energy criterion thermodynamically for the uphill reactions involved in water splitting.

The electrode potential of Ag/Ag_3PO_4 is between the reduction potential of H^+ and $Ag/AgNO_3$ (Fig. 2a; ref. 19), which means Ag_3PO_4 cannot split water to release H_2. It is, however, a potential photofunctional material possessing strong photooxidative capabilities in the presence of the sacrificial reagent silver nitrate. O_2 evolution over Ag_3PO_4 in an aqueous silver nitrate solution under visible-light irradiation was therefore tested. The typical amount of evolved O_2 as a function of time is shown in Fig. 2b. For comparison purposes, the performance of two recognized light-sensitive semiconductors for O_2 evolution, $BiVO_4$ (prepared according to ref. 20) and WO_3 (Commercial, Wako; ref. 21), under the same experimental conditions, are also shown. It was found that Ag_3PO_4 is the highest performing, with vigorous bubbles of O_2 being observed as soon as light irradiation commenced (Supplementary Movie S1).

The wavelength dependence of the O_2 evolution was then further investigated to prove whether or not the reaction really was driven by light[11,12]. Figure 2c shows the ultraviolet–visible diffuse reflectance spectrum of the Ag_3PO_4 along with the apparent quantum yield of O_2 evolution as a function of the incident light wavelength. The apparent quantum yield decreased with increasing wavelength and the longest wavelength suitable for O_2 evolution was found to coincide with the absorption edge of the semiconductor Ag_3PO_4. This indicates that the oxygen
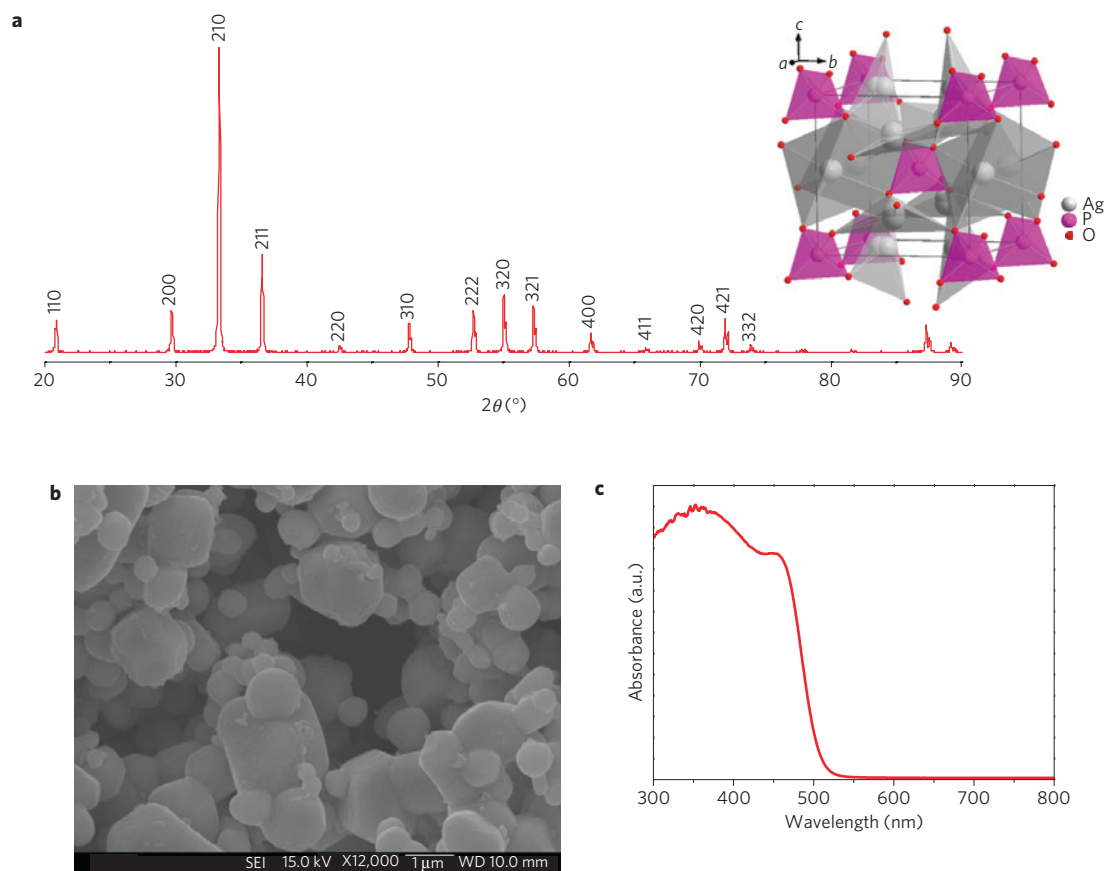
Figure 1 | Crystal structure, particle morphology and optical property of Ag₃PO₄. a, XRD patterns of the Ag_3PO_4 powders. Inset: Schematic drawing of the crystal structure. **b**, SEM image of the prepared Ag_3PO_4 powders. **c**, Ultraviolet–visible diffusive reflectance spectrum of the Ag_3PO_4 samples.

evolution reaction is indeed driven by light and that the light absorption property of the semiconductor governs the reaction rate. The extremely high quantum yield at wavelengths less than ∼480 nm, significantly higher than previously reported values[7,10–12,20], shows that the recombination of photoexcited electrons and holes within the material is very weak.

In consideration of the knowledge that silver salts are well known to decompose on light irradiation, supplementary experiments such as pure water splitting and ^{18}O-isotope-labelled water oxidation and so on (see Supplementary Experimental S1, Fig. S2 and Table S1), were also carried out and the results confirm that the oxygen observed is without doubt derived from the oxidation of water.

Organic dye decomposition[9,22,23] experiments using silver nitrate as an electron acceptor were also carried out to further certify the strong photooxidative ability of the semiconductor. Figure 2d(I) shows the variation of methylene blue concentration with illumination time over Ag_3PO_4(Brunauer–Emmett–Teller (BET), $0.98\,m^2\,g^{-1}$). For comparison purposes, the results of methylene blue decomposition over monoclinic $BiVO_4$ (BET, $1.2\,m^2\,g^{-1}$), commercial $TiO_{2-x}N_x$ (BET, $43\,m^2\,g^{-1}$) and methylene blue photolysis under the same conditions (see the Methods section and Supplementary Fig. S3) are also shown. It was found that the process of methylene blue decomposition over Ag_3PO_4 was dozens of times quicker than that over the reference materials. It is noted here that only ∼14% of the methylene blue was adsorbed on the Ag_3PO_4 powders when equilibrium adsorption states were reached during the dark reaction and the pH value of the solution was kept constant (the pH of deionized water) during the reaction. This shows once again that Ag_3PO_4 has very high photooxidation activity indeed. The inset in Fig. 2d(I) shows the colour changes of the methylene blue solutions during the photooxidation process.

In view of the fact that organic dyes can also harvest visible light, experiments with methylene blue photodegradation over Ag_3PO_4 powders under different monochromatic visible-light irradiation conditions were designed to test the possibly evolved effects of photosensitization (Fig. 2d(II)). From ultraviolet–visible absorption spectra (see Supplementary Fig. S4) it is clear that the methylene blue dyes are most excited by a wavelength of approximately 600–700 nm and least excited by a wavelength of 350–500 nm, whereas the Ag_3PO_4 semiconductors can be excited only by a wavelength shorter than ∼530 nm, as described above. Therefore, we first used monochromatic visible light centred at a wavelength of 420.4 nm ($\Delta\lambda = \pm 14.9$ nm) to excite the Ag_3PO_4 semiconductor but minimize the excitation of the methylene blue. The methylene blue was still exhausted very quickly. In contrast, when monochromatic visible light centred at a wavelength of 639.3 nm ($\Delta\lambda = \pm 16.2$ nm) was used to excite the methylene blue molecules but not the Ag_3PO_4 semiconductor, it is difficult to observe any methylene blue degradation at all. The effect of photosensitization during methylene blue decomposition over Ag_3PO_4 is thus negligible. In other words, methylene blue decomposition can definitely be attributed to the intrinsic strong photooxidative activity of the Ag_3PO_4.

It is worth mentioning that even without sacrificial reagent the Ag_3PO_4 still shows strong photooxidative ability (see Supplementary Figs S2a and S5). The results of total organic carbon (TOC) measurements as well as decomposition experiments using other organic compounds (see Supplementary Fig. S6) indicate that the strong photooxidative ability of Ag_3PO_4 is also effective in these cases.

Unfortunately, as the electrode potential of Ag/Ag_3PO_4 is lower than that of the hydrogen electrode the Ag_3PO_4 semiconductor
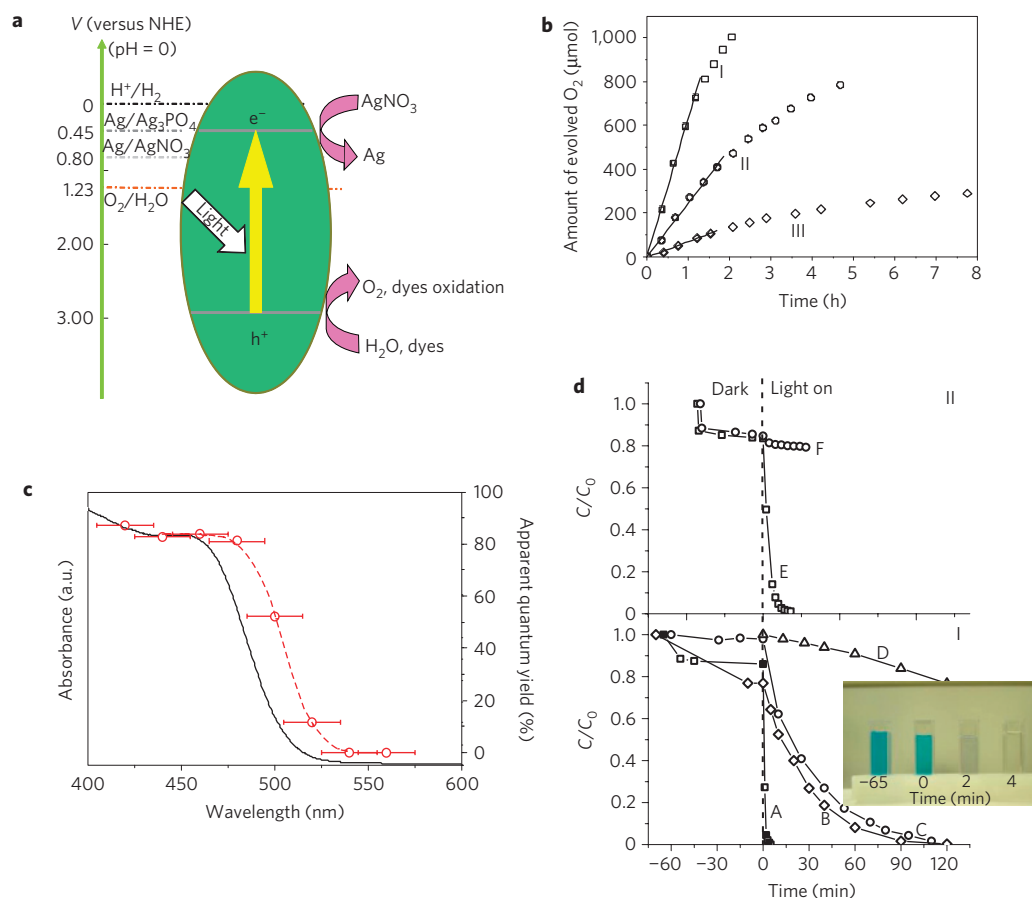
Figure 2 | Photooxidation over Ag₃PO₄ under visible light. a, Schematic drawing of redox potentials of Ag_3PO_4. **b**, O_2 evolution from aqueous $AgNO_3$ solutions under illumination ($\lambda > 400$ nm) on various semiconductor powders, respectively. (I) Ag_3PO_4: 636 µmol h⁻¹; (II) $BiVO_4$: 246 µmol h⁻¹; (III) WO_3: 72 µmol h⁻¹. **c**, Ultraviolet–visible diffuse reflectance spectrum and apparent quantum yields of the Ag_3PO_4 semiconductor plotted as a function of wavelength of the incident light. Apparent quantum yields were plotted at the centre wavelengths of the band-pass filters, with error bars showing the deviation of the wavelengths ($\Delta\lambda = \pm15$ nm). **d**, Variation of methylene blue concentration as a function of illumination time (with the time of light on set as 0) under visible light ($\lambda > 400$ nm) (I) with powder samples Ag_3PO_4 (A), $TiO_{2-x}N_x$ (B), $BiVO_4$ (C) and methylene blue photolysis (D), and under various monochromatic visible lights with Ag_3PO_4 (II) at wavelengths of $\lambda = 420.4$ nm ($\Delta\lambda = \pm14.9$ nm) (E) and $\lambda = 639.3$ nm($\Delta\lambda = \pm16.2$ nm)(F). The inset shows the colour changes of the methylene blue solutions corresponding to the four filled square points in A.

would decompose during the water oxidation if no sacrificial reagent was involved (see Supplementary Fig. S7). Silver phosphate decomposition can, however, be halted or delayed. Inspired by the facts that: (1) the aforementioned redox scheme can be viewed as a short-circuited photoelectrochemical cell[24]; and (2) water oxidization on the Ag₃PO₄ semiconductor occurs automatically once it is illuminated ($\lambda < 530$ nm), we designed a macroscopic photoelectrochemical cell (see Supplementary Fig. S8) in which Ag₃PO₄ thin films deposited onto an inert conducting substrate are used both as a water oxidization reactor and as the macroscopic electrode when halting/delaying the process of photocorrosion or restoring the material is needed. The latter function is warranted by adding a solar cell as an alternative to the sacrificial reagent. The difference in the electrode potential between Ag/Ag⁺ and O₂/H₂O justifies the cell configuration.

Figure 3a shows an SEM image of the *in-situ*-deposited Ag₃PO₄ thin film. Cyclic voltammetry was used to investigate the effect of light on the current density (Fig. 3b), in terms of the photocurrent and dark-current response from the sample. The positive photocurrent at anodic potentials suggests that the Ag₃PO₄ electrode is an n-type semiconductor. The onset potential of this semiconductor electrode is 0.9–$1.0V_{\mathrm{NHE}}$. The dark current is very weak up to about $1.3V_{\mathrm{NHE}}$, where electrocatalytic oxygen evolution starts. The proven contribution of light irradiation to the current

density between 1.0 and $1.3V_{\mathrm{NHE}}$ indicates that the Ag₃PO₄ thin film can be used positively as a photoanode. As Ag₃PO₄ oxidizes water automatically while simultaneously itself being reduced under light irradiation ($4Ag_3PO_4 + 6H_2O + 12h^+ + 12e^- \rightarrow 12Ag + 4H_3PO_4 + 3O_2$), a change in irradiation conditions also changes the state of the photoelectrode. That is why the onset potential shows slight variation in Fig. 3b. Moreover, the bias voltage here can be set either to transfer the photoexcited electrons to the external circuit or to re-oxidize the reduced Ag. The incident photo-to-current efficiency here (see Supplementary Fig. S9) is therefore an indirect measure of the ability to delay the photocorrosion, instead of a measure of oxygen evolution activity.

As well-crystallized Ag₃PO₄ semiconductor can form at room temperature, in an aqueous solution containing silver cations and phosphate anions, the sample preparation method contains an inbuilt rejuvenation mechanism; that is, when the fabricated Ag₃PO₄ thin films decompose during prolonged illumination (in practical operation, some of the photoexcited electrons reduce the silver instead of being transferred to the external circuit owing to the semiconductive feature of the photoelectrode), the reduced Ag would deposit onto the inert conducting substrate whereas the phosphate anions would go into aqueous solution, as found in the analyses of the samples of the solution after water splitting (see Supplementary Figs S2b and S7c). The Ag₃PO₄
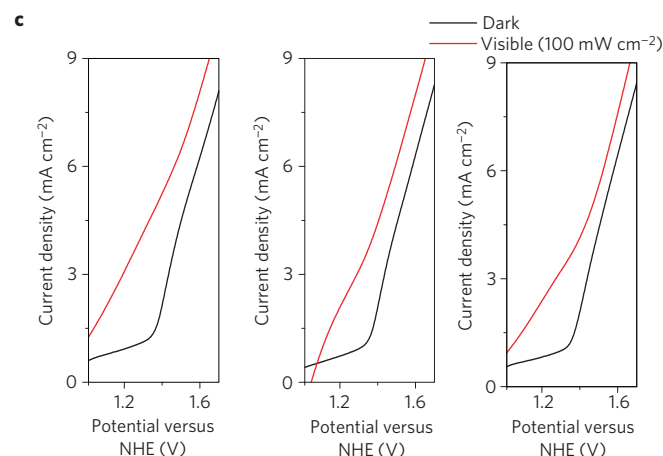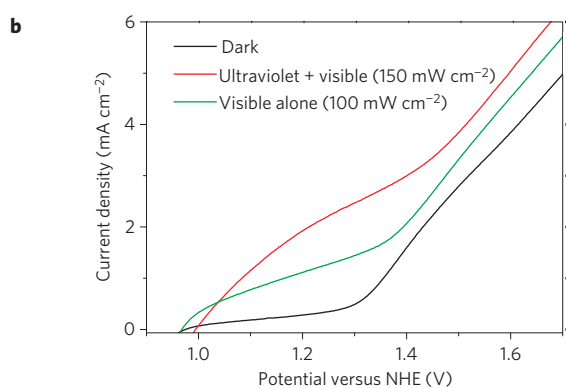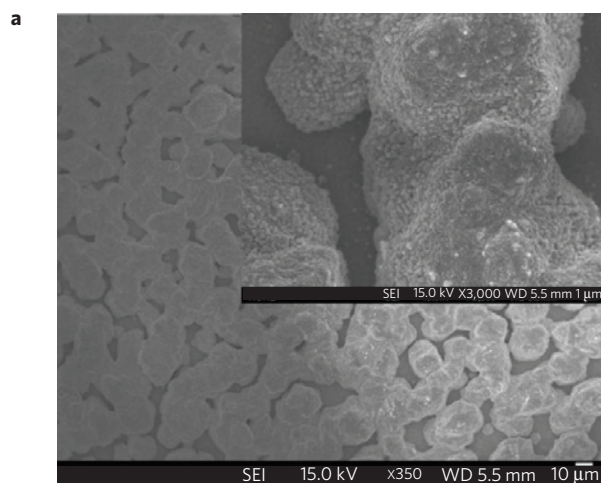
Figure 3 | Photoelectrochemistry of Ag₃PO₄. **a**, SEM images of the deposited Ag_3PO_4 thin films. **b**, Current density versus potential curves for a Ag_3PO_4-coated ITO glass photoelectrode in 0.02 M Na_3PO_4 under different illumination conditions. **c**, Photocurrent and dark-current response for the Ag_3PO_4 thin films rejuvenated after every 30 h illumination.

thin films can therefore be restored *in situ* by anodic oxidation. Figure 3c shows the photocurrent and dark-current response for the Ag_3PO_4 thin films rejuvenated after every 30 hours illumination. Optimization of the photoelectrochemical cell system, involving the control of film thickness, contact resistance, particle size, surface morphology, cell configuration and so on, is still needed, to improve performance (see Supplementary Movie S2). The most important point, however, is that this photoelectrochemical cell configuration
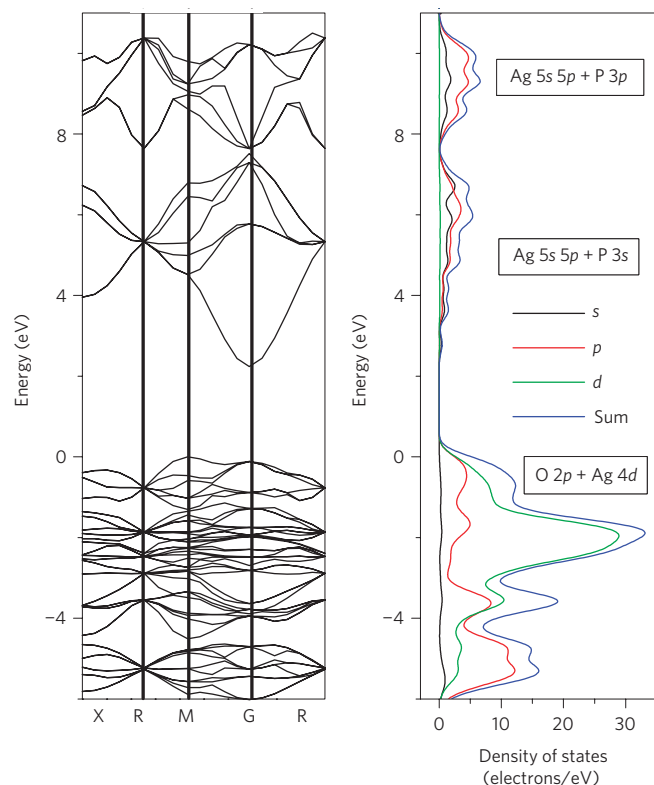

Figure 4 | Energy-band diagram and density of states for Ag₃PO₄ calculated by a density functional method.

makes the Ag_3PO_4 semiconductor function in sunlight without using sacrificial reagents.

To obtain further insight into the high photooxidative activity of Ag_3PO_4, *ab initio* density functional theory (DFT) calculations have also been carried out. Although the bandgap from DFT calculations is usually underestimated, they nonetheless often provide important insight into the physicochemical behaviour of the materials investigated. Figure 4 shows the energy-band dispersion and density of states of Ag_3PO_4 calculated using CASTEP (ref. 25). The material is an indirect bandgap semiconductor, as has been revealed from the absorption spectrum. The direct gap at the Gamma point and the indirect gap are energetically very close together, which explains the features of the measured absorption spectrum (see Supplementary Fig. S1) as well as the very steep rise in photocurrent. Both the highly dispersive valence bands and conduction bands should be beneficial for the transport of photoexcited electrons and holes. This in turn is likely to suppress the recombination of electron–hole pairs and thus account for the high photooxidative activity. It is important to note that the bottoms of the conduction bands are mainly composed of hybridized Ag $5s5p$ as well as a small quantity of P $3s$ orbitals, whereas the tops of the valence bands are composed of hybridized Ag $4d$ and O $2p$ orbitals. It is known that Ag_2O is a narrow-bandgap semiconductor with a black colour. The addition of phosphorus in the case of Ag_3PO_4 seems to adjust both the band structure and the redox power and thereby results in the high photooxidation by Ag_3PO_4 under visible-light irradiation. The calculated optical property shows that the absorption edge is in agreement with the experimentally measured edge (see Supplementary Fig. S10).

The electronic band structure considerations also suggest a strategy in the design of new photoelectrode materials, that is, start from a binary oxide of narrow bandgap (for example, Ag_2O, Bi_2O_3, PbO, Cu_2O, Fe_2O_3, Cr_2O_3, V_2O_5 and so on) and try to add *p* block elements and/or alkali or alkaline earth ions in such a way as to

change the crystal structure (thereby, adjusting the bandgap and the redox power). Some photoelectrode materials that fulfil this strategy are listed in Supplementary Table S2.

Methods

Sample preparation. Powder samples were prepared by the ion-exchange method: appropriate amounts of raw powders of Na_2HPO_4 (or Na_3PO_4) and $AgNO_3$ were thoroughly mixed until the initial white colour changed to yellow. The mixture was then washed with distilled water to dissolve any unreacted raw material. Last, the vivid yellow powders obtained were dried at 70 °C in air overnight. Thin films were prepared by an electrochemical method: first, a piece of indium–tin-oxide (ITO)-coated glass (1 cm × 2 cm) as the cathode and a piece of Pt sheet as the anode were immersed in a 0.02 M silver nitrate solution with 1.0 V d.c. voltage to deposit a bright layer of Ag on the conducting glass surface. Then the anode and the cathode of the d.c. power source were exchanged and the electrolyte was replaced by a 0.02 M sodium orthophosphate solution. The Ag on the surface of the ITO glass was gradually oxidized and reacted with orthophosphate anions *in situ* to form vivid yellow Ag_3PO_4 thin films under a d.c. voltage of 0.8–0.9 V. The rejuvenation process is just as the fabrication of the thin films, that is, oxidizing the reduced Ag *in situ* in the sodium orthophosphate solution with a d.c. voltage of 0.8–0.9 V.

Physical characterization. The crystal structures were determined by XRD using Cu Kα radiation (Rigaku, RINT-2100). The ultraviolet–visible diffuse reflectance spectra were measured using the diffuse reflection method with a Shimadzu UV-2500 spectrophotometer. Then the absorption spectra were obtained from the reflectance spectra by means of Kubelka–Munk transformations. Particle sizes and surface morphology were observed with a field-emission SEM. Specific surface areas of samples were measured by the BET method (N_2 adsorption) with a Gemini-2360 instrument (Micrometrics, Shimadzu).

Oxygen evolution and apparent quantum yield. The Ag_3PO_4 powders (0.5 g) were dispersed by a magnetic stirrer in 270 ml of H_2O in a Pyrex reaction cell. $AgNO_3$ (0.85 g) was added for the experiments involving sacrificial reagent. The light source was an ozone-free 300 W Xe arc lamp (Hayashi Tokei, Luminar Ace 210). A cutoff filter of 420 nm was employed for the visible-light irradiation. The light intensity of the oxygen evolution reactions was measured by a spectroradiometer (Ushio, USR-40). The apparent quantum yields at various wavelengths were measured by inserting a water filter and various band-pass filters in front of the reaction cell to get the desired incident wavelength. At the same time, the light intensity was tuned to minimize diffusive reflection of the incident light. The amount of evolved O_2 was determined using a gas chromatograph (Shimadzu, GC-8A, TCD, Ar carrier) and the apparent quantum yield was obtained from the percentage of the number of reacted electrons during O_2 evolution to the number of incident photons.

Organic dye decomposition. The photoinduced decomposition of the organic dyes was carried out with 0.3 g of the Ag_3PO_4 powders suspended in a dye solution (15.3 mg l^{-1}, 100 ml), prepared by dissolving the organic powders in distilled water in a Pyrex glass cell. $AgNO_3$ (0.3 g) was added to scavenge the photoexcited electrons for the experiments involving sacrificial reagent. The optical system for the degradation reaction included a 300 W Xe lamp, a cutoff filter of 420 nm and a water filter (to prevent infrared irradiation). Before illumination the suspensions were magnetically stirred in the dark for ~40 min to ensure establishment of an adsorption/desorption equilibrium of dyes on the sample surfaces. The experiments were carried out at room temperature in air. The pH of the solutions was kept constant (at ~7.0) during the reactions. The suspensions including the sample powders and dyes were sampled every few minutes. The sample powders were then separated by centrifuging and the dye solutions were analysed. The concentration of the organic dyes was determined by monitoring the height of the maximum of the absorbance in ultraviolet–visible spectra and the TOC content in the aqueous solutions was analysed using a TOC analyser (TOC-V CPH, Shimadzu).

Photoelectrochemistry characterization. The photoelectrochemical properties were investigated in a conventional three-electrode cell by using an electrochemical analyser (Model-650A). The Ag_3PO_4-coated ITO glass, a piece of Pt sheet, a Ag/AgCl electrode and 0.02 M sodium orthophosphate were used as the working electrode, the counter-electrode, the reference electrode and the electrolyte, respectively. Cyclic voltammograms were collected at 0.1 V s^{-1} and at a sensitivity of 0.002 A V^{-1}. The light source was a 500 W Xe lamp. A cutoff filter of 420 nm was employed for the visible-light irradiation and the light intensity was tuned to one Sun (100 mW cm^{-2}). The incident photo-to-current efficiency (IPCE) was obtained with the formula of IPCE = $(1241 \times I_{ph})/(p \times \lambda)$, where p and λ are the intensity (μW cm^{-2}) and the wavelength (nm) of the incident monochromatic light, respectively. I_{ph} is the photocurrent density (μA cm^{-2}). The different wavelengths of incident monochromatic light were generated by band-pass filters whereas the light intensity was measured with a spectroradiometer (Ushio, USR-40). During the IPCE measurement the lamp current was kept at 20 A.

First-principles calculations. The calculations were carried out using the local density approximation. Ultrasoft pseudopotentials were applied with a plane-wave cutoff energy of 340 eV. The valence electronic configurations for Ag, P and O are $4d^{10}5s^1$, $3s^23p^3$ and $2s^22p^4$, respectively. The primitive unit cell is composed of $[Ag_3PO_4]_2$, and the number of occupied orbitals is 62. Scissors of 2.0 eV and smearing of 0.5 eV were employed for the results analysis.

References

1. Fujishima, A. & Honda, K. Electrochemical photolysis of water at a semiconductor electrode. *Nature* **238**, 37–38 (1972).
2. Metzner, H., Fischer, K., Strasser, R. & Schnell, G. in *Proc. Int. Congr. Photosyn. Res.* 2nd edn, Vol. 1 (ed. Priestley, J.) 359–362 (1972).
3. Lewis, N. S. Light work with water. *Nature* **414**, 589–590 (2001).
4. Lewis, N. S. & Nocera, D. G. Powering the planet: Chemical challenges in solar energy utilization. *Proc. Natl Acad. Sci. USA* **103**, 15729–15737 (2006).
5. Kanan, M. W. & Nocera, D. G. In situ formation of an oxygen-evolving catalyst in neutral water containing phosphate and Co^{2+}. *Science* **321**, 1072–1075 (2008).
6. Wang, X. C. *et al.* A metal-free polymeric photocatalyst for hydrogen production from water under visible light. *Nature Mater.* **8**, 76–80 (2009).
7. Zou, Z. G., Ye, J. H., Sayama, K. & Arakawa, H. Direct splitting of water under visible light irradiation with an oxide semiconductor photocatalyst. *Nature* **414**, 625–627 (2001).
8. Yamashita, H. *et al.* Degradation of propanol diluted in water under visible light irradiation using metal ion-implanted titanium dioxide photocatalysts. *J. Photochem. Photobiol. A* **148**, 257–261 (2002).
9. Asahi, R., Morikawa, T., Ohwaki, T., Aoki, K. & Taga, Y. Visible light photocatalysis in nitrogen doped titanium oxides. *Science* **293**, 269–271 (2001).
10. Ishikawa, A. *et al.* Oxysulfide Sm$_2$Ti$_2$S$_2$O$_5$ as a stable photocatalyst for water oxidation and reduction under visible light irradiation. *J. Am. Chem. Soc.* **124**, 13547–13553 (2002).
11. Maeda, K. *et al.* Photocatalyst releasing hydrogen from water. *Nature* **440**, 295 (2006).
12. Tsuji, I., Kato, H. & Kudo, A. Visible-light-induced H$_2$ evolution from an aqueous solution containing sulfide and sulfite over a ZnS–CuInS$_2$–AgInS$_2$ solid-solution photocatalyst. *Angew. Chem. Int. Ed.* **44**, 3565–3568 (2005).
13. Khaselev, O. & Turner, J. A. A monolithic photovoltaic–photoelectrochemical device for hydrogen production via water splitting. *Science* **280**, 425–427 (1998).
14. Grätzel, M. Photoelectrochemical cells. *Nature* **414**, 338–344 (2001).
15. Saladin, F., Kamber, I., Pfanner, K. & Calzaferri, G. Photochemical water oxidation to oxygen at the solid/gas interface of AgCl on zeolite A. *J. Photochem. Photobiol. A* **109**, 47–52 (1997).
16. Helmholz, L. The crystal structure of silver phosphate. *J. Chem. Phys.* **4**, 316–322 (1936).
17. Ng, H. N., Calvo, C. & Faggiani, R. A new investigation of the structure of silver orthophosphate. *Acta Crystallogr. B* **34**, 898–899 (1978).
18. Masse, R., Tordjman, I. & Durif, A. Refinement of crystal structure of silver monophosphate, Ag$_3$PO$_4$—existence of high-temperature form. *Z. Kristallogr.* **114**, 76–81 (1976).
19. Bard, A. J., Parsons, R. & Jordan, J. *Standard Potentials in Aqueous Solution* P306 (CRC Press, 1985).
20. Kudo, A., Omori, K. & Kato, H. A novel aqueous process for preparation of crystal form-controlled and highly crystalline BiVO$_4$ powder from layered vanadates at room temperature and its photocatalytic and photophysical properties. *J. Am. Chem. Soc.* **121**, 11459–11467 (1999).
21. Erbs, W., Desilvestro, J., Borgarello, E. & Grätzel, M. Visible light induced O$_2$ generation from aqueous dispersions of WO$_3$. *J. Phys. Chem.* **88**, 4001–4006 (1984).
22. Arai, T. *et al.* The enhancement of WO$_3$-catalyzed photodegradation of organic substances utilizing the redox cycle of copper ions. *Appl. Catal. B* **84**, 42–47 (2008).
23. Li, X. K., Kikugawa, N. & Ye, J. H. Nitrogen-doped lamellar niobic acid with visible light responsive photocatalytic activity. *Adv. Mater.* **20**, 3816–3819 (2008).
24. Bard, A. J. Photoelectrochemistry and heterogeneous photocatalysis at semiconductors. *J. Photochem.* **10**, 59–75 (1979).
25. Segall, M. D. *et al.* First-principles simulation: Ideas, illustrations and the CASTEP code. *J. Phys. Condens. Matter.* **14**, 2717–2743 (2002).

Author contributions

Z.Y. fabricated the samples, designed the study, carried out XRD, SEM, ultraviolet–visible spectra, BET, O_2 evolution, quantum yield, organic dyes decomposition, electrochemistry experiments, DFT calculations and related data analysis, and wrote the paper; J.Y. supervised the research work and discussed the results; N.K. carried out the TOC analysis; T.K. offered the $BiVO_4$ samples and carried out the HPLC analysis; S.O. contributed part of the DFT calculations; H.S-W. carried out the ^{18}O isotope analysis; H.Y. directed the electrochemistry experiments; J.C. contributed part of the electrode fabrication; W.L. and Z.L. carried out part of the photocurrent measurement; Y.L. helped with the photoelectrode fabrication; R.L.W. discussed the results and polished the English.

Additional information